

---

# Princeton Plasma Physics Laboratory

---

PPPL-

PPPL-



Prepared for the U.S. Department of Energy under Contract DE-AC02-09CH11466.

# Princeton Plasma Physics Laboratory

## Report Disclaimers

---

### Full Legal Disclaimer

This report was prepared as an account of work sponsored by an agency of the United States Government. Neither the United States Government nor any agency thereof, nor any of their employees, nor any of their contractors, subcontractors or their employees, makes any warranty, express or implied, or assumes any legal liability or responsibility for the accuracy, completeness, or any third party's use or the results of such use of any information, apparatus, product, or process disclosed, or represents that its use would not infringe privately owned rights. Reference herein to any specific commercial product, process, or service by trade name, trademark, manufacturer, or otherwise, does not necessarily constitute or imply its endorsement, recommendation, or favoring by the United States Government or any agency thereof or its contractors or subcontractors. The views and opinions of authors expressed herein do not necessarily state or reflect those of the United States Government or any agency thereof.

### Trademark Disclaimer

Reference herein to any specific commercial product, process, or service by trade name, trademark, manufacturer, or otherwise, does not necessarily constitute or imply its endorsement, recommendation, or favoring by the United States Government or any agency thereof or its contractors or subcontractors.

---

## PPPL Report Availability

### Princeton Plasma Physics Laboratory:

<http://www.pppl.gov/techreports.cfm>

### Office of Scientific and Technical Information (OSTI):

<http://www.osti.gov/bridge>

---

### Related Links:

[U.S. Department of Energy](#)

[Office of Scientific and Technical Information](#)

[Fusion Links](#)

## Lithium wall conditioning and surface dust detection on NSTX

C.H. Skinner<sup>a,\*</sup>, J.P. Allain<sup>b</sup>, M.G.Bell<sup>a</sup>, F.Q.L. Friesen<sup>c</sup>, B. Heim<sup>b</sup>, M.A. Jaworski<sup>a</sup>,  
H. Kugel<sup>a</sup>, R. Maingi<sup>d</sup>, B. Rais<sup>e</sup>, C.N. Taylor<sup>b</sup>.

<sup>a</sup>Princeton Plasma Physics Laboratory, Princeton, NJ 08543, USA

<sup>b</sup>Purdue University, West Lafayette, 400 Central Drive, IN 47907, USA

<sup>c</sup>Grinnell College, 1115 8th Avenue, Grinnell, IA 50112 USA

<sup>d</sup>Oak Ridge National Laboratory, Oak Ridge, Tennessee 37831, USA

<sup>e</sup>Université de Provence, Aix-Marseille, PACA 13001, France

### Abstract

Lithium evaporation onto NSTX plasma facing components (PFC) has resulted in improved energy confinement, and reductions in the number and amplitude of edge-localized modes (ELMs) up to the point of complete ELM suppression. The associated PFC surface chemistry has been investigated with a novel plasma-material interface probe connected to an *in-vacuo* surface analysis station. Analysis has demonstrated that binding of D atoms to the polycrystalline graphite material of the PFCs is fundamentally changed by lithium – in particular deuterium atoms become weakly bonded near lithium atoms themselves bound to either oxygen or the carbon from the underlying material.

Surface dust inside NSTX has been detected in real-time using a highly sensitive electrostatic dust detector. In a separate experiment, electrostatic removal of dust via three concentric spiral-shaped electrodes covered by a dielectric and driven by a high voltage 3-phase waveform was evaluated for potential application to fusion reactors.

*[147 words, limit 150 words]*

PACS numbers: 34.35.+a, 52.40.Hf, 52.55.Fa, 52.90.+z

Corresponding author: Charles Skinner email: [cskinner@pppl.gov](mailto:cskinner@pppl.gov)

## 1. Introduction

Plasma facing materials in fusion reactors face serious issues with respect to their erosion lifetime, tritium inventory control, limits on plasma contamination, damage from off-normal events, radiation damage, and helium blistering [1]. Although in ITER the plasma facing materials are not seriously challenged by neutron damage, the same materials may not be suitable for the radiation environment of a fusion power reactor. Because they can, in principle, be replenished, liquid materials are more tolerant of radiation damage, helium blisters and erosion. Their possible applications to fusion were reviewed in ref. [2]. As a plasma facing material, liquid lithium has the further potential advantage of binding with hydrogen isotopes, thereby reducing recycling of the plasma efflux from the PFCs. This can dramatically enhance plasma performance as was first seen in TFTR for lithium applied to graphite[3], and then on other machines [4,5]. Lithium surfaces can potentially offer divertor pumping over a large area compatible with high flux expansion solutions for power exhaust. We report here on the latest applications of lithium to diverted plasmas in National Spherical Torus Experiment (NSTX).

The formation of large amounts of radioactive and chemically active dust are expected in next step fusion devices because of the intense plasma-wall interactions and long pulse durations. There are administrative and safety limits on the dust inventory in the ITER vessel [6] to address concerns on public safety and vacuum vessel integrity, and to minimize plasma contamination and the degradation of diagnostic mirrors. However the development of methods to measure surface dust in remote and inaccessible areas in tokamaks remains in its infancy [7]. Electrostatic detectors [8] offer a promising approach to monitoring conductive dust in areas such as underneath the divertor dome in ITER where dust accumulation is likely to occur. The first real-time measurement of surface dust in the NSTX tokamak was reported in ref. [9]. Very high signals were observed when lithium particles were injected for wall conditioning purposes. In this paper we describe the development of an *in-situ* helium puffer to clear residual dust from the detector while still in the vacuum vessel, and the investigation of an electrostatic dust “conveyor” that might be applied to controlling the dust inventory in a tokamak.

## 2. Li conditioning of NSTX

NSTX produces low aspect ratio, neutral beam heated, diverted plasmas with a typical major radius of 0.85 m and minor radius 0.65 m [10]. The plasma facing surfaces are mostly ATJ<sup>TM</sup> graphite tiles. Two lithium evaporators can be inserted at the top of the vessel and evaporate lithium at a rate of 5 – 70 mg/min onto the lower plasma facing components between discharges [11]. Lithium has a low ionization potential and the prompt ionization of incoming lithium together with a large (60%) secondary ion emission factor [12] lead to a very low influx of lithium into the main plasma. On NSTX core lithium concentrations ( $n_{Li}/n_D$ ) are typically 0.1% or less. Before the introduction of lithium, intershot helium glow discharge cleaning was used to maintain density control. With lithium conditioning this became unnecessary, giving an additional benefit of 40% more discharges per week of operations.

### 2.1 NSTX plasma performance with lithium

Lithium absorbs and sequesters atomic hydrogen species, reducing the recycling flux from the graphite PFCs. After evaporation of lithium onto NSTX PFCs the deuterium gas fuelling needed to reach a given average density increased compared to pre-lithium values, while the deuterium Balmer- $\alpha$  line emission decreased, despite the increased gas puffing, indicating reduced deuterium recycling [13]. This recycling reduction is accompanied by a pronounced modification of the edge plasma profiles, as shown in Fig. 1. First the edge electron density gradient is reduced in the H-mode transport barrier region [14]. Interpretive modelling [15] with the 2-D b2/EIRENE code package has shown that this profile change occurs due to reduced core fuelling as a result of the reduced recycling at the divertor plates and a drop in the edge particle transport rate. The reduced edge density is accompanied by an edge  $T_e$  increase, partly to maintain approximately constant plasma pressure and partly due to a decrease in the edge electron thermal transport. The drop in density reduces the collisional coupling between the electrons and ions, allowing the edge ion  $T_i$  to increase also. Finally the drop in edge neutral density due to lower recycling leads to reduced charge-exchange momentum loss, and a higher edge rotation speed.

These dramatic changes in the edge profiles are also thought to be responsible for the suppression of edge localized modes (ELMs) in H-mode plasmas. The reduction in the average edge density gradient, and its movement inward from the separatrix reduced the local bootstrap current, which is driven by the density and temperature gradients. This reduction of near-separatrix bootstrap current is stabilizing to kink/peeling modes, which are thought to be responsible for ELMs in NSTX. Detailed stability analysis confirms that the discharges with lithium are further from the kink/peeling boundary than the ELMy discharges. However in most cases the suppression of ELMs leads to the accumulation of carbon impurities in the core plasma toward the end of the plasma pulse, although this impurity build-up may be reduced by the application of pulses of non-axisymmetric radial field perturbations that reintroduce controlled ELMs [16].

The time dependent transport analysis code TRANSP has confirmed that mid-radius electron thermal transport is progressively reduced as lithium deposition increases [17]. In addition, the fast-ion contribution to the total energy increased. The core thermal ion confinement remains close to the neoclassical level, both with and without lithium.

Before the 2010 experimental campaign, a molybdenum Liquid Lithium Divertor (LLD) was installed in NSTX as a step toward providing long-pulse pumping of deuterium in a liquid lithium volume [18,19]. The plasma facing surface of the LLD has a 0.17 mm thick layer of molybdenum plasma sprayed to produce a porosity of 45% onto a protective barrier of 0.25mm stainless steel, bonded to a 22 mm thick copper substrate. The porosity is intended to take advantage of the high surface tension of lithium to facilitate wetting and to stabilize the lithium layer against electromagnetic forces. The porous surface was filled with lithium with the two lithium evaporators. The LLD plates were heated both electrically and by the plasma energy outflow to temperatures up to 320°C (the melting temperature of lithium is 180°C) and the porous surface was filled with lithium with the two lithium evaporators. In plasma operation with the divertor strike point incident on the LLD no significant molybdenum influx into the plasma was observed and the LLD withstood direct exposure to the heat flux from the outer strike point ( $\sim 5 \text{ MW/m}^2$  for  $\sim 0.5 \text{ s}$ ). The beneficial effects of lithium on plasma performance were reproduced with the LLD. However, the deuterium fuelling needed to maintain a reference

discharge did not increase when the LLD surface temperature increased above the lithium melting temperature suggesting that there was no significant change in deuterium pumping provided by the liquid surface.

## 2.2 Lithium surface chemistry in fusion devices.

Both graphite and lithium can bind with the deuterium plasma efflux making it unavailable for recycling. Prompt retention of 87% of the deuterium fuel gas has been measured at the end of NSTX neutral beam heated discharges and this number increased to 93% with lithium applied [20]. A significant increase in the wall deuterium inventory was found in lithium conditioned discharges. The deuterium is retained in complex chemical bonds with carbon, lithium, oxygen, and other impurities. Changes in surface morphology due to ion bombardment and the difficulty of diagnosis of plasma facing surfaces, especially reactive surfaces complicate the development of a predictive understanding of the wall and its interaction with the plasma. Evaporated lithium can react with residual gases in the vacuum chamber before a discharge. On NSTX, lithium evaporation is performed in the intershot interval when outgassed water vapor is typically pumped from  $3 \times 10^{-6}$  Torr to  $4 \times 10^{-7}$  Torr. At this point the evaporator is withdrawn and the NB cryopump valve is opened to bring the pressure down to  $4 \times 10^{-8}$  Torr before the next discharge. During evaporation, the time for a monolayer of lithium to impinge on the divertor surface is comparable to the surface monolayer formation time (6 s) at a water pressure of  $4 \times 10^{-7}$  Torr. Additional issues in surface chemistry include segregation of buried or dissolved impurities to the surface of molten lithium [21] and intercalation of lithium into graphite [22]. Key factors for long pulse deuterium pumping are the saturation of deuterium in lithium [23], diffusion of deuterium away from the plasma-facing surface and the hydrogen binding abilities of lithium-based materials that have become contaminated with plasma impurities.

To gain insights into the surface chemistry underlying deuterium retention, a probe was installed on NSTX that exposed 4 samples to the lower divertor plasma. The probe and samples were then withdrawn *in-vacuo* into an attached chamber for thermal desorption spectroscopy (TDS) analysis [20]. The samples were then retrieved under argon for additional TDS and X-ray photoelectron analysis (XPS) in the Omicron surface analysis laboratory at Purdue University [24]. The analysis revealed that the binding of D atoms on a graphite surface is fundamentally

changed by lithium – in particular hydrogen atoms are weakly bonded in regions near lithium atoms bound to either oxygen or the carbon matrix [25]. There was an interesting correlation of dependence of the XPS peaks on lithium deposition and an increased difference in deuterium retention with increased lithium deposition. The prompt release after a discharge of the additional deuterium retained with lithium may be understood in the light of the low energy D bonding peak found in the TDS spectra. Fig. 2 illustrates aspects of the surface chemistry of porous molybdenum (as used for the LLD) and graphite surfaces after evaporation of lithium and deuterium irradiation. Curves (a, e) show a similar XPS peak positioned near 533 eV for both the Mo and ATJ graphite samples that, for lithiated graphite, is attributed to Li-O-D interactions [24]. However the Mo sample represented in curve (b) does not exhibit the typical Li-O-D surface chemistry (with a peak located at 533 eV) that is seen in lithiated ATJ graphite following D irradiation, but instead more closely resembles lithiated graphite *prior* to D irradiation. This apparent lack of Li-O-D interactions suggests that D is diffusing into the bulk Li within the Mo porosity [26].

This year a more advanced “materials analysis particle probe” (MAPP) is being installed on the NSTX vessel to investigate the relationship between lithium conditioned surface composition and plasma behaviour. It will have capability to perform TDS, XPS and direct recoil spectroscopy (DRS) analysis of samples promptly after exposure to NSTX plasmas. Other lithium related technologies under development at PPPL include high heat flux testing of lithium-bearing components, a molten lithium delivery system for the LLD and a lithium particle dropper designed to provide the capability to continually replenish lithium on plasma facing surfaces during a discharge [27,28].

### **3. Electrostatic detection and removal of surface dust**

Local measurements of surface dust are planned in ITER to provide information on pulse-by-pulse dust generation and to help manage the dust inventory. A measurement requirement of 20% relative and 50% absolute accuracy has been specified [29]. However dust measurement techniques are still in their infancy, especially for dust on hot surfaces. Electrostatic detection of dust on remote surfaces was first demonstrated in 2004 using two closely interlocking combs of copper traces on a circuit board that were biased to 50 V [30]. Conductive dust particles settling

on the detector cause an electrical breakdown between adjacent traces and the resulting current pulse was detected electronically. At the same time the heat generated by the current caused the particles to rocket off the surface or vaporize, thus restoring an open circuit. The first laboratory tests achieved a threshold sensitivity of  $50 \mu\text{g}/\text{cm}^2$ . This was about four orders of magnitude above the amount of dust falling during one pulse in contemporary tokamaks. However the detector sensitivity has now been increased by the required factor by decreasing the gap between the traces, increasing the detector size, and by refinements in the detection electronics. The threshold sensitivity of the 5 cm x 5 cm detector to carbon particles in vacuum is now  $0.15 \text{ ng} / \text{cm}^2 / \text{count}$ . A smaller 1.2 x 1.2 cm detector was tested with the lithium particles of  $44 \mu\text{m}$  mean diameter and the sensitivity in vacuum without mesh cover was measured to be  $14.5 \text{ ng} / \text{cm}^2 / \text{count}$ . The results for lithium “dust” may be considered as a proxy for beryllium (occupational safety concerns have inhibited experiments with beryllium dust). The first real-time measurements of surface dust in NSTX were recently reported in ref. [9].

Disruptions appear to be a significant source of dust in NSTX. Of the 20 discharges with the highest dust signals, 15 discharges (75%) underwent plasma disruptions (defined by a change in stored energy of  $>50 \text{ kJ}$  at plasma termination) or a significant internal reconnection event. This is a much higher fraction than the 16% overall disruption frequency for this data set. An electrostatic dust detector has also been installed on Tore Supra with on-line measurement of the amplitude and duration of the dust signals. Dust detection events on Tore Supra also often coincident with disruptions and in particular the amount of dust detected has been correlated with the severity of the disruption [31].

### *3.1 Residual dust removal via helium puff*

Typically more than 90% of the total number of particles that land on the dust detector are vaporized by the current pulse and ejected from the detector; however, laboratory measurements have indicated that up to 10% may remain on the detector surface [32]. These may produce additional breakdowns between the traces at a later time, complicating efforts to correlate a tokamak dust signal with plasma events.

A helium puff system was developed to clear from the detector any residual dust, debris or fibers that might cause a permanent short. The system incorporated a small  $5.2 \text{ cm}^3$  plenum that

was pressurized with 6 bar of helium and exhausted into a vacuum chamber via high flow rate pneumatic valves that are compatible with the magnetic field environment of a tokamak[33,34]. A manifold with three 0.45 mm nozzles at an angle of 30° to a horizontal surface was able to visibly clear a 5 cm x 5 cm area (the size of the detector) as shown in Fig. 3. Small residual amounts of microscopic dust particles may not be detectable in the images but none-the-less can be monitored by the operation of the detector. Any residual dust on the detector can be disturbed by the helium puff or a mechanical knock producing breakdown between the energized traces and a detectable current pulse. The procedure to test the efficiency of the puff system was to perform a sequence of helium puffs and mechanical knocks and observe any resulting counts. Fig. 4 shows the percentage of additional counts that occurred after successive puff and knock events. It can be seen that the first puff could trigger about 3% of additional counts followed by about 1% due to a knock on the chamber. Subsequent puffs after the first two, caused less than 0.5% of additional counts indicating that two puffs were sufficient to almost entirely clear the surface of the detector of residual dust. Some particles could be held up on a cover mesh that was intended to prevent large ( $> 90 \mu\text{m}$ ) particles from reaching the detector. A 4<sup>th</sup> nozzle aimed at the mesh was able to clear it in the same puff. As measured by the dust detector itself, two helium puffs were able to reduce residual dust on the detector to less than 0.01% of the incident particles. The system is designed to be compatible with NSTX as the valves are non-magnetic and the quantity of gas used is similar to that used to fuel the NSTX plasmas and would be quickly pumped by the NSTX vacuum pumping system.

### *3.2 Electrostatic dust removal*

The ability to manage inventories of carbon, tritium, and high-Z dust in fusion plasmas depends on means for effective dust removal from the tokamak. Currently ITER plans to use a remotely operated vacuum cleaner to remove accumulated dust during periodic divertor exchanges while its vacuum vessel is vented. However, more advanced dust removal technology will be needed in future fusion reactors, as the amount of dust generated increases with the duty cycle and the time available to remove it is correspondingly reduced. The concept of an ‘electrostatic curtain’ to remove dust from surfaces was proposed during the Apollo lunar missions [35], and dust transport aimed toward fusion applications was reported in ref. [36].

However, this system required high voltage (22 kV) and the space needed was prohibitive for ITER. A smaller scale dust conveyor has been previously developed by NASA to clear dust from lunar solar cells [37], and the application of this device to removal of fusion-relevant dust was investigated.

The NASA dust conveyor utilizes three concentric spiral-shaped indium tin oxide electrodes driven by a 3-phase waveform and is shown in Fig. 5. The waveforms create a series of electrostatic potential wells that sweep radially across the conveyor to move charged particles. Insulating particles can acquire charge through dielectrophoresis and/or through triboelectrification (from rubbing on either the dielectric surface covering the electrodes or other particles). Conducting particles can become charged through induction charging. The peak-to-peak waveform amplitude was up to 3,000 V and the driving frequency was varied from 5 Hz to 210 Hz [38].

Visual observations of the dust conveyor showed that large ( $\sim 10 \text{ mm}^3$ ) volumes of carbon and tungsten dust dropped on the surface could be efficiently cleared within 5 s. Image analysis was used to obtain quantitative measurements of the particle size distribution and the quantity present on the conveyor at a given time. The amount of dust was limited so that individual particles and clumps of particles were visibly separated and differences in removal efficiency would be clearly revealed. Small glass spheres and sand were also used to provide a basis for comparison with the conductive carbon and tungsten particles. The conveyor removed material most rapidly during the first several steps (a single step refers to the period of time in which two of the three driving phases change state once, and the remaining phase changes state twice). Fig. 6 shows the cumulative amount of material removed by the conveyor for each material after every step. Rapid removal of tungsten particles is seen after about 5 steps. The removal rate data for carbon is complicated by an increase in apparent volume as large clumps of particles are broken up by the application of the electric field [38].

Significant development work remains before either the detector or conveyor devices could be operated reliably for long periods without maintenance in the harsh ITER in-vessel environment including fabrication from radiation resistant materials. As the dust levels of

concern in ITER are much higher than the levels in existing tokamaks a less sensitive detector with thicker, more rugged traces would be appropriate and a ruggedized detector for tungsten dust is under development. For electrostatic dust removal in a fusion device we envision a mosaic of dust conveyors that would transport dust accumulating in hidden areas on the lower vacuum vessel into exhaust ports. The conveyors would utilize contemporary advances in micro- and nano- technology, and be based on linear arrays that would generate the required travelling electric field with low voltages applied to more closely spaced traces. A limited demonstration of electrostatic dust motion with 25  $\mu\text{m}$  spaced traces operated at 50 V was reported in ref. [39].

#### **4. Summary**

Lithium conditioning of NSTX plasma facing components has reduced recycling, suppressed ELMs, and increased the stored energy of diverted plasmas. A valuable benefit has been a 40% increase in the number of discharges per week of operations as helium glow discharge cleaning between successive discharges is no longer needed. A Liquid Lithium Divertor was installed in 2010 as a step toward providing long-pulse pumping of deuterium in a liquid lithium volume and has functioned well. However any additional deuterium pumping was masked by the large existing pumping by the surrounding lithiated graphite. Links between the plasma behaviour and the chemistry of lithiated surfaces have been found using a novel on-vessel surface analysis diagnostic.

Electrostatic detection of surface dust has been demonstrated in NSTX. A helium puffer to remove residual dust from the detector has been developed and electrostatic removal of fusion relevant dust has been demonstrated in the laboratory as a first step toward dust management in fusion reactors.

#### **Acknowledgement**

We thank C. Calle of the NASA Electrostatics and Surface Physics Laboratory, Kennedy Space Center, FL for supplying the dust conveyor used in sect. 3.3. We acknowledge stimulating discussions with B. Koel and L Roquemore and thank the NSTX team for expert technical assistance. This work is funded by U.S. DOE Contract No. DE-AC02-09CH11466

## Figure Captions

Figure 1. Effect of lithium on NSTX edge profiles of (a) electron temperature, (b) ion temperature, (c) electron density and (d) toroidal velocity. The data are from shots 129014 @ 0.555s - no lithium (○) and 129061 @ 0.695s - with lithium (Δ). Both shots have the same 6 MW neutral beam heating power and the same fuelling. The times were selected to match the line averaged electron density of  $5.5 \times 10^{13} \text{ cm}^{-3}$ . The lines are a visual aid.

Figure 2. XPS O1s spectra showing changes in surface chemistry with D irradiation of Li deposited on cold, hot, C contaminated Mo and graphite. (a) is after 30 minutes of D<sub>2</sub> irradiation on 2 microns of Li deposited on cold Mo; (b) after 30 minutes D<sub>2</sub> irradiation on 2 microns of Li at 255 °C- the Li was deposited on cold Mo; (c) after 30 minutes D<sub>2</sub> irradiation on 3 microns Li at 200 °C – Li deposited on Mo at 250°C; (d) carbon sputtered (via Ar) onto Li-coated Mo – 30 min D<sub>2</sub> irradiation at 200 °C; (e) after 30 minutes D<sub>2</sub> irradiation on ATG Graphite with 2 micron nominal Li coat.

Figure 3. Images of carbon particles in air at atmospheric pressure taken with a digital camera (a) before puff and (b) after a helium puff. Puffing was performed with a three-nozzle manifold with a 30° incidence angle and 6 bar plenum pressure.

Figure 4. Percentage of additional counts triggered by consecutive puffs labeled 1P, 2P, 3P ... and knocks labeled 1K, 2K, 3K ... in vacuum conditions without cover mesh and with the 3 nozzles manifold. For three trials the percentage of additional counts triggered by a knock event after a second puff was lower than 0.5%.

Figure 5. Schematic of voltage waveforms (on left) applied to a 44 mm diameter spiral pattern of three indium tin oxide traces on a glass substrate. A thin insulating PET cover film prevented electrical breakdown between the traces. The waveform amplitude is  $2V_A$  and a ‘precharge’ voltage  $V_{PC}$  can also be applied.

Figure 6 Volume removed vs. step number for tungsten (◆ solid diamonds), carbon (● solid circles), glass (Δ open triangles) and sand particles (X). The conveyor was operated a 500 V pre-charge voltage for 10 s for all materials, followed by single steps of peak to peak voltage amplitude roughly optimized for each material as follows: 2750 V for tungsten, 2000 V for carbon, 3000 V for glass and sand. There was an interval of about 20 s between each step for photographic imaging.

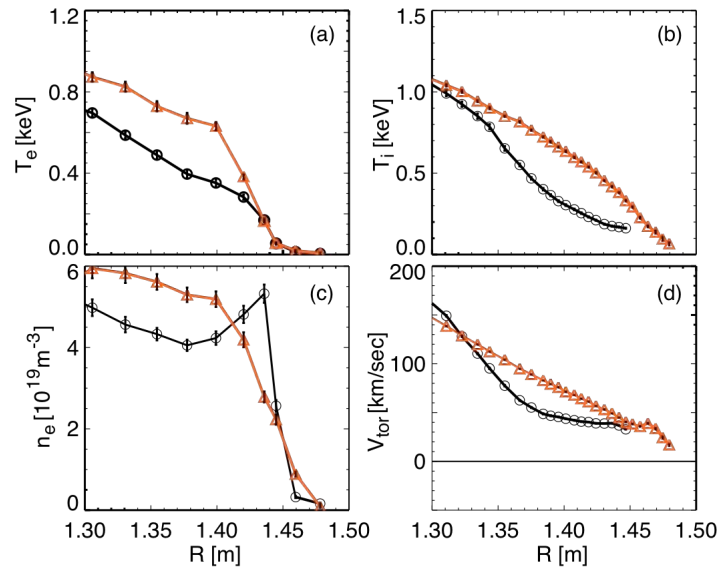


Figure 1. Effect of lithium on NSTX edge profiles of (a) electron temperature, (b) ion temperature, (c) electron density and (d) toroidal velocity. The data are from shots 129014 @ 0.555s - no lithium ( $\circ$ ) and 129061 @ 0.695s - with lithium ( $\Delta$ ). Both shots have the same 6 MW neutral beam heating power and the same fuelling. The times were selected to match the line averaged electron density of  $5.5 \times 10^{13} \text{ cm}^{-3}$ . The lines are a visual aid.

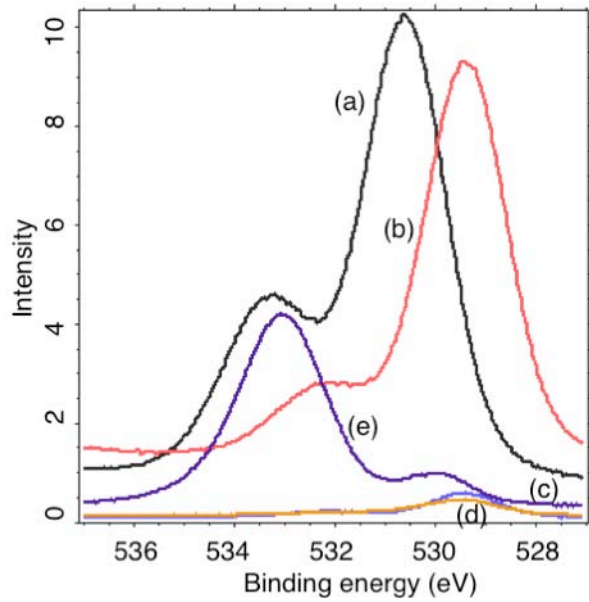
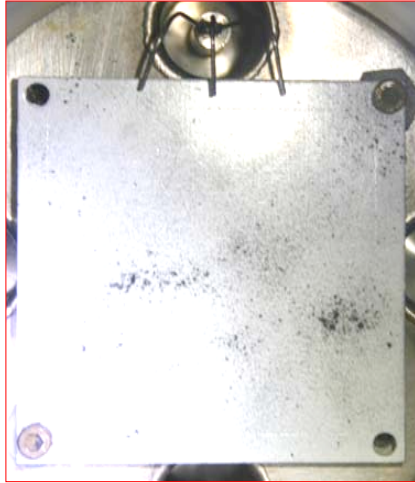


Figure 2 XPS O1s spectra showing changes in surface chemistry with D irradiation of Li deposited on cold, hot, C contaminated Mo and graphite. (a) is after 30 minutes of D<sub>2</sub> irradiation on 2 microns of Li deposited on cold Mo; (b) after 30 minutes D<sub>2</sub> irradiation on 2 microns of Li at 255 °C- the Li was deposited on cold Mo; (c) after 30 minutes D<sub>2</sub> irradiation on 3 microns Li at 200 °C – Li deposited on Mo at 250°C; (d) carbon sputtered (via Ar) onto Li-coated Mo – 30 min D<sub>2</sub> irradiation at 200 °C; (e) after 30 minutes D<sub>2</sub> irradiation on ATG Graphite with 2 micron nominal Li coat.

(a)



(b)

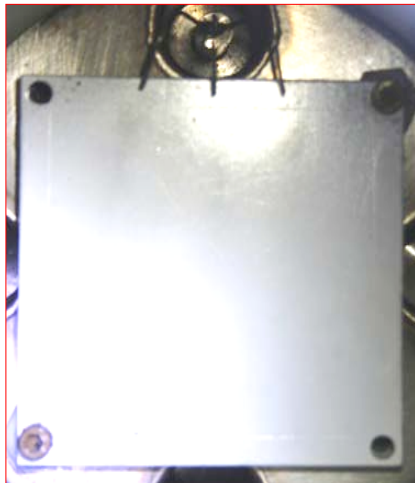


Figure 3. Images of carbon particles in air at atmospheric pressure taken with a digital camera (a) before puff and (b) after a helium puff. Puffing was performed with a three-nozzle manifold with a  $30^\circ$  incidence angle and 6 bar plenum pressure.

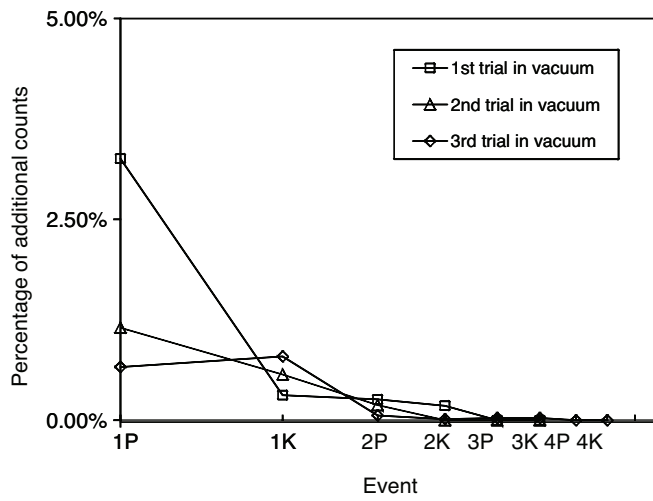


Figure 4 Percentage of additional counts triggered by consecutive puffs labeled 1P, 2P, 3P ... and knocks labeled 1K, 2K, 3K ... in vacuum conditions without cover mesh and with the 3 nozzles manifold. For three trials the percentage of additional counts triggered by a knock event after a second puff was lower than 0.5%.

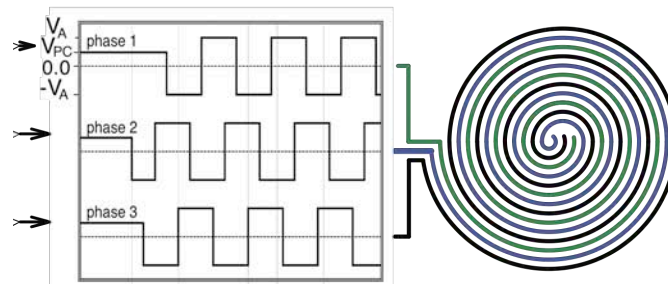


Figure 5 Schematic of voltage waveforms (on left) applied to a 44 mm diameter spiral pattern of three indium tin oxide traces on a glass substrate. A thin insulating PET cover film prevented electrical breakdown between the traces. The waveform amplitude is  $2V_A$  and a 'precharge' voltage  $V_{PC}$  can also be applied.

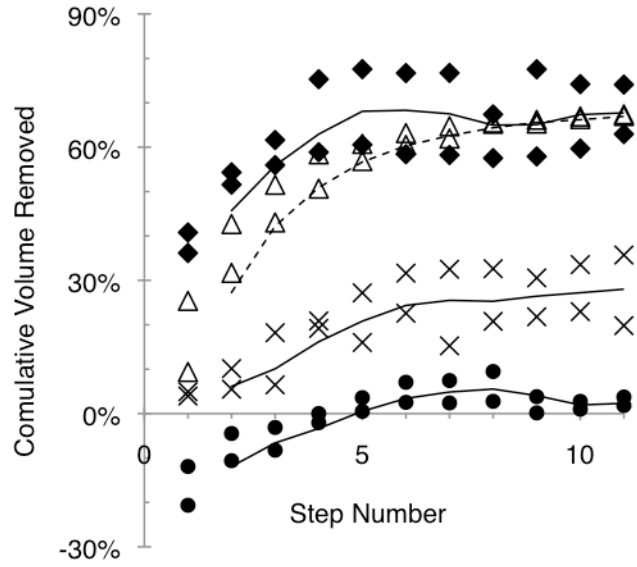


Figure 6 Volume removed vs. step number for tungsten (♦ solid diamonds), carbon (● solid circles), glass (Δ open triangles) and sand particles (X). The conveyor was operated a 500 V pre-charge voltage for 10 s for all materials, followed by single steps of peak to peak voltage amplitude roughly optimized for each material as follows: 2750 V for tungsten, 2000 V for carbon, 3000 V for glass and sand. There was an interval of about 20 s between each step for photographic imaging.

## References

- [1] G. Federici, 2006 *Phys. Scr.* **T124** 1.
- [2] R. F. Mattas et al., 2000 *Fus. Eng. & Des.*, **49-50** 127.
- [3] D. K. Mansfield, *et al.*, 2001 *Nucl. Fusion* **41** 1823.
- [4] R. Kaita et al., 2007 *Phys. Plasmas*, **14** 056111.
- [5] Proceedings of the 1st International Workshop on Lithium Applications for the Boundary Control in Fusion Devices, *Fus. Eng. Des.*, Volume **85** 837-962 (November 2010)
- [6] S. Rosanvallon et al., 2009 *J. Nucl. Mater.*, **390-391** 57-60
- [7] D. L. Rudakov et al., 2008 *Rev. Sci. Instrum.*, **79** 10F303
- [8] C. H. Skinner et al., 2004 *Rev. Sci. Instrum.* **75** 4213
- [9] C. H. Skinner et al., 2010 *Rev. Sci. Instrum.*, **81** 10E102.
- [10] M.G. Bell et al., 2009 *Plasma Phys. Control. Fus.* **51** 124056.
- [11] H. W. Kugel et al., 2010 *Fus. Eng. & Des.*, **85** 865.
- [12] J.P. Allain, M.D. Coventry and D.N. Ruzic, 2007 *Phys. Rev. B* **13** 056117
- [13] H. W. Kugel et al., 2011 *J. Nucl. Mater.*, at press.
- [14] R Maingi et al., 2009 *Phys. Rev. Lett.*, **103** 075001
- [15] J.M. Canik et al., 2011 *Phys. Plasmas* at press.
- [16] J.M. Canik et al., 2010 *Phys. Rev. Lett.* **104** 045001.
- [17] S. Ding et al., 2010 *Plasma Phys. Control. Fusion* **52** 015001
- [18] H. W. Kugel et al., 2011 Proceedings of 23rd IAEA Fusion Energy Conference, 11-16 October 2010, Daejeon, Rep. of Korea, *Nucl. Fus.* at press.
- [19] H. W. Kugel et al., 2011 “NSTX Plasma Operation with a Liquid Lithium Divertor” Proceedings of the 2nd International Symposium on Lithium Applications for Fusion Devices April 27-29, 2011, Princeton, NJ, USA to be published in *Fus. Eng. & Des.*
- [20] C. H. Skinner et al., 2011 *J. Nucl. Mater.*, at press.
- [21] R. Bastasz and J.A. Whaley, 2004 *Fus. Eng. & Des.*, **72** 111.
- [22] N. Itou et al., 2001 *J. Nucl. Mater.*, **290-293** 281.
- [23] M.J. Baldwin et al., 2002 *Nucl. Fus.*, **42** 1318.

- [24] C. N. Taylor, B. Heim, J.P. Allain., 2011 *J. Appl. Physics* **109** 052206.
- [25] C. N. Taylor et al., 2011 *J. Nucl. Mater.*, at press.
- [26] B. Heim, et al., 2011 J.P. Allain., *Nucl. Instr. and Meth. B*  
doi:10.1016/j.nimb.2011.01.001
- [27] D. K. Mansfield et al., 2010 *Fus. Eng. and Des.* **85** 890–895
- [28] A.L. Roquemore, et al., 2011 “Techniques for injection of pre-characterized dust into the scrape-off layer of fusion plasma”, *Fusion Eng. Des.*, doi:10.1016/j.fusengdes.2011.02.053
- [29] ITER\_Diagnostic\_Project\_Requirements\_(PR)\_27ZRW8\_v4\_0.
- [30] A. Bader et al., 2004 *Rev. Sci. Instrum.* **75** 370.
- [31] 'First results from dust detection during plasma discharges in Tore Supra' Poster P26A H.Roche et al., these proceedings.
- [32] C. V. Parker, C. H. Skinner, and A. L. Roquemore, 2007 *J. Nucl. Mater.* **363–365**, 1461.
- [33] B. Rais, C. H. Skinner, and A. L. Roquemore, 2011 *Rev. Sci. Instrum.*, **82** 036102.
- [34] ‘Advances in Dust Detection for Tokamaks’ B. Rais et al., Poster P27A this conference.
- [35] F.B. Tatom, V. Srepel, R.D. Johnson, N.A. Contaxes, J.G. Adams, H. Seaman, and B.L. Cline, “Lunar Dust Degradation Effects and Removal/Prevention Concepts”, NASA Technical Report No. TR-792-7- 207A, p. 3-1 (1967).
- [36] M. Onozuka et al., 1997 *J. Nucl. Sci and Technol.* **34** 1031.
- [37] C.I. Calle et al., 2009 *Journal of Electrostatics* **67** 89–92.
- [38] F.Q.L. Friesen et al., 2011 C.I. Calle, *Rev. Sci. Instrum.*, at press.
- [39] A. Campos and C.H. Skinner, 2009 *Journal of Undergraduate Research* vol. IX 30.  
[http://www.scied.science.doe.gov/scied/JUR\\_v9/default.htm](http://www.scied.science.doe.gov/scied/JUR_v9/default.htm)

The Princeton Plasma Physics Laboratory is operated  
by Princeton University under contract  
with the U.S. Department of Energy.

Information Services  
Princeton Plasma Physics Laboratory  
P.O. Box 451  
Princeton, NJ 08543

Phone: 609-243-2245  
Fax: 609-243-2751  
e-mail: [pppl\\_info@pppl.gov](mailto:pppl_info@pppl.gov)  
Internet Address: <http://www.pppl.gov>